Author/s:
Hassan, S;Ekanayake, NIK;Scales, PJ;Batterham, RJ;Stickland, AD

Title:
Quantifying the effect of ultra-fine particles on dewatering performance in bimodal suspensions

Date:
2025-05-31

Citation:
Hassan, S., Ekanayake, N. I. K., Scales, P. J., Batterham, R. J. & Stickland, A. D. (2025). Quantifying the effect of ultra-fine particles on dewatering performance in bimodal suspensions. Powder Technology, 458, pp.1-11. https://doi.org/10.1016/j.powtec.2025.120986.

Persistent Link:
https://hdl.handle.net/11343/355998

Powder Technology 458 (2025) 120986

Contents lists available at ScienceDirect

Powder Technology

journal homepage: www.journals.elsevier.com/powder-technology

Quantifying the effect of ultra-fine particles on dewatering performance in bimodal suspensions

Sajid Hassan, Nilanka I.K. Ekanayake, Peter J. Scales, Robin J. Batterham, Anthony D. Stickland *

ARC Centre of Excellence for Enabling Eco-Efficient Beneficiation of Minerals, Department of Chemical Engineering, The University of Melbourne, Victoria 3010, Australia

HIGHLIGHTS

- Systematically quantifying ultra-fine particles' impact on dewatering processes.
- Ultra-fine particles are detrimental to filtration processes.
- Increasing ultra-fine content decreases dewatering extent and permeability.
- Filter press modelling compares filtration performance with minimal samples.
- Solids throughput decreases, but filtration area/time increases with ultra-fines.

GRAPHICAL ABSTRACT

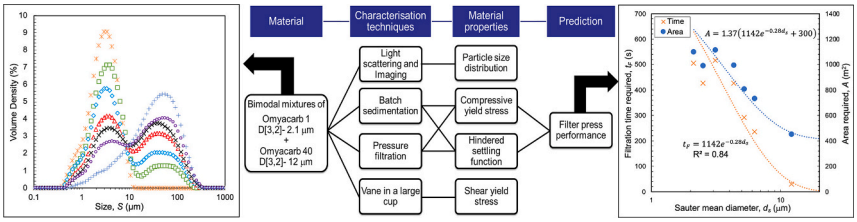

ARTICLE INFO

Keywords:
Compressional rheology
Cake permeability
Filtration
Shear
Particle packing

ABSTRACT

A systematic approach was employed to evaluate and quantify the impact of ultra-fine particles on dewatering processes. Model suspensions were created by incorporating calcium carbonate particles of two distinct sizes (2.1 µm and 12.2 µm Sauter mean diameter) to simulate various levels of ultra-fine content. The objective was to compare differences based solely on particle size while maintaining consistent surface chemistry characteristics.

As the ultra-fine content increased from 0 % to 100 %, the gel point decreased linearly from 38 v/v% to 22 v/v %, permeability decreased by up to 40 times, shear yield stress increased by 100 times, and extent of dewatering decreased from 63 v/v% to 53 v/v% at 600 kPa pressure. However, in specific blends, the dewatering extent exceeded expectations, whereby beyond a certain compressive load, the data is consistent with the optimal packing of smaller particles into the voids between the coarser particles. Furthermore, the impact of altering compressibility and permeability on dewatering was quantified using a numerical filter press model, highlighting the sensitivity of dewatering to the content of ultra-fine particles.

The filtration time decreases exponentially with increasing Sauter mean diameter, following the relationship $t_F = 1142\exp(-0.28d_s)$. Additionally, the filtration area is linearly related to the filtration time, as shown by the equation $A = 1.37(t_F + 300)$.

* Corresponding author.
E-mail address: stad@unimelb.edu.au (A.D. Stickland).

https://doi.org/10.1016/j.powtec.2025.120986
Received 29 September 2024; Received in revised form 23 March 2025; Accepted 26 March 2025
Available online 29 March 2025

1. Introduction

1.1. Overview

Filtration is the preferred solid-liquid separation method for achieving low moisture contents across various industries, including wastewater treatment, mineral processing, pharmaceuticals, oil and gas, pulp and paper processing, chemical processing and food processing [1–4]. It is particularly crucial for suspensions with fine and ultra-fine particles, where gravitational separation is inadequate.

In mineral processing, the depletion of higher-grade ores and the increasing demand for minerals driven by population growth, urbanisation, and the green technology revolution [5–7] have led to increased extraction from lower-grade ores and finer grinding [6,8–14]. This results in increased production of fine mineral tailings, posing significant challenges for solid-liquid separation processes [15]. Inadequate separation leads to less efficient recycling of process water and potential risks to the geotechnical safety of tailings storage facilities (TSFs).

Thickeners are often used as the final dewatering step because of their cost-effectiveness; however, the heightened focus on water recovery, driven by scarcity in many mining locations and the need to adhere to environmental regulations, has increased interest in high-pressure filtration devices like filter presses. Achieving higher solids concentration is crucial, but this goal may prove challenging in systems with high fine content, even with rigorous high-pressure filtration. A systematic approach is needed to quantify these dewatering limitations consistently and repeatedly without the significant costs associated with pilot-scale assessments.

1.2. Filtration theory

Dewatering processes, like filtration, increase the solid concentration of a suspension, resulting in the observation of non-Newtonian flow behaviour [16]. The theoretical framework of compressional rheology, developed by Buscall and White [17], describes filtration performance using two key material functions: the compressive yield stress and the hindered settling function.

In filter presses, the attainment of high solid concentrations necessitates the application of elevated pressures. This applied pressure, ΔP, will match the compressive yield stress, $P_y(\phi)$, which is the suspension resistance to consolidation due to interparticle network strength [18]. At equilibrium at a constant applied pressure, the suspension reaches a specific solids volume fraction, defined by $P_y(\phi)$, which quantifies its compressibility. The gel point, ϕ_g, marks the critical solids volume fraction at which particles can self-assemble into a supportive structure. Below ϕ_g, $P_y(\phi)$ is zero, as the particulates are too dilute to facilitate interparticle interactions and the formation of a space-filling and stress-bearing particle network. Beyond ϕ_g, the network resists consolidation until an external differential pressure surpasses $P_y(\phi)$, prompting liquid release and a subsequent increment increase in solids volume fraction. Additionally, the hindered settling function, $R(\phi)$, reflects the hydrodynamic drag of liquid flowing past particles and is inversely correlated with the dewatering rate [18]. At low ϕ, $R(\phi)$ is low, indicating minimal flow resistance and rapid dewatering. Conversely, at high ϕ, $R(\phi)$ increases sharply as reduced pore space creates greater resistance to flow.

The compressibility and permeability of suspensions are highly non-linear functions of solids concentrations, making dewatering behaviour difficult to predict using single dewatering parameters alone. Skinner et al. [19] showed that due to the interdependent nature of compressibility and permeability, differences in dewatering behaviour between two particulate suspensions cannot be easily scaled based on single parameters. Instead, validated models of dewatering devices, such as filter presses, provides a quantitative comparison and enable scenario planning for changes in process conditions and feed types.

1.3. Impact of particle properties on filtration

Particle size distribution, shape, and interparticle interactions [3,4,20–22] are key factors that influence the compressibility, permeability, and shear rheology of suspensions [23–25].

Coarse particles, characterised by larger pores, facilitate rapid fluid flow due to increased permeability. Conversely, fine particles impede fluid flow due to more surface area and stronger particle interactions [26]. In binary mixtures, rheological studies have shown that there is not a linear transition between a coarse to fine rich mixture since a characteristic packing sequence emerges. Coarse particles initially establish a densely packed structure, subsequently allowing finer particles to fill the voids, increasing packing density [27]. However, after reaching an optimal packing density, further addition of fine particles leads to a reduction in packing density until it aligns with that of the fine particle mixture [28]. Consequently, an ideal mixture exists where fine particles effectively occupy interstitial voids within the coarser matrix, optimising packing density. This effect is especially pronounced when the fine-to-coarse ratio approaches 10, which has been shown to maximise packing efficiency [29]. Research also indicates that under fixed pressure conditions, optimal packing occurs when fine particles make up about 30 % of the total volume [29,30], or fall within the range of 15 % to 20 % [31]. However, in real-world suspensions, which often have diverse particle size distributions, the dewatering behaviour becomes more complex.

Particle shape and interparticle interactions also play a crucial role in packing arrangement and density [32]. Smaller, non-spherical particles typically have more surface area and friction [33], which influences packing density. While plates and needles without interparticle interactions can theoretically pack to higher densities than spherical particles, spherical particles typically exhibit higher packing efficiency than non-spherical ones due to these surface area dependent interactions [4,34]. Complexity escalates when materials harbour a mix of particle shapes, as the combination can induce interlocking or bridging phenomena, influencing packing density either positively or negatively, contingent upon specific shapes and their proportions.

Interparticle interactions, such as van der Waals and electrostatic forces, can intricately modulate optimum packing and rheological traits within the system, as documented by Dinger and Funk [27]. For instance, suspensions with high zeta potential have strong repulsive forces that prompt particles to disperse, with individual particles integrating into the filter cake at concentrations approximating random close packing [30]. However, this phenomenon is not mirrored in many mineral tailings suspensions containing fine particles with net attractive interparticle potential, resulting in a continuous particulate network at lower packing fractions that resists consolidation. Notably, suspensions exhibiting higher viscosity typically stem from weaker repulsive forces and the formation of particle networks [35], underscoring a crucial trade-off in dewatering systems between the degree and speed of dewatering.

The shear yield stress, $\tau_y(\phi)$, is the stress required to make a concentrated suspension flow like a liquid rather than deform like a solid. Previous investigations have demonstrated that the shear yield stress increases with an increasing proportion of fines for a given solids volume fraction [28]. As the coarser fraction increases, shear yield stress decreases because the large particles occupy more space, reducing surface area per unit volume. The gel point and equilibrium packing fraction of fine particles also increase with more coarse particles, reaching a maximum value before declining to that of the coarse particles [28]. This fluctuation highlights that increasing fines necessitate elevated compressive loads to disrupt the solid network and expel the entrapped liquid.

Ultimately, the interplay between particle size, shape, distribution, and interparticle interactions determines key dewatering properties, including permeability, compressibility, and shear rheology. Although previous research has extensively investigated sand-fine systems

[23,24,28,30,31,36], the role of ultra-fines—particles below 5 μm—remains largely unaddressed. Ultra-fines significantly impede dewatering processes but a comprehensive understanding of their effect on compressibility and permeability across different solids concentrations is still lacking.

1.4. Study purpose

This study aims to systematically investigate the role of ultra-fine particles in bimodal suspensions and quantify their impact on dewatering performance using a simple laboratory methodology. While acknowledging that multiple factors may influence dewatering performance, our focus in this study is confined to exploring the impact of particle size and ratio alone at a constant state of aggregation and without changes in particle shape.

To this end, we selected two distinct sizes of calcium carbonate particles (2.1 μm and 12.2 μm Sauter mean diameter) and blended them in various proportions with water to create model suspensions. These two sizes were selected as it can represent a wide range of fine mineral tailings. Although a size ratio of roughly 10 has been associated with optimal packing of strictly bidisperse distributions, real-world suspensions often exhibit broader distributions. Different particle size selections could shift observed trends, particularly in compressibility and permeability.

To evaluate dewaterability, these suspensions were characterised for compressibility, permeability, and shear yield stress. Filter press modelling was used to predict filtration performance, focusing on how ultra-fine content influences filtration time, required filtration time, and achievable solids throughput. By establishing functional relationships between particle size and dewatering performance, this study provides a framework for optimising filtration processes in industrial applications without requiring expensive pilot-scale trials.

Unlike previous studies that primarily focus on mono-sized suspensions or coarse-fine mixtures with limited ultra-fine content, this study systematically quantifies the impact of ultra-fine particles across a wide range of solid concentrations. The findings contribute novel insights into the interactions between compressibility, permeability and shear behaviour in bimodal suspensions, offering practical considerations for managing ultra-fine content in mineral tailings dewatering. These insights can inform filtration strategies to enhance water recovery and improve solid-liquid separation processes in industrial applications.

2. Materials and methods

2.1. Overview

To quantify the dewaterability of suspensions containing varying quantities of ultra-fine particles using minimal samples, this study utilised blends of two distinct particle sizes of calcium carbonate (Omyacarb 1 and Omyacarb 40, provided by Omya Australia Pty Ltd.). The impact of bimodal particle distributions on compressional and shear rheological properties was investigated, and the resulting changes in filter press performance were analysed.

The experimental methodology overview, illustrated in Fig. 1, encompassed four distinct techniques for characterising the bimodal calcium carbonate mixtures. These techniques included particle size analysis, batch sedimentation, pressure filtration, and determination of shear yield stress using the vane-in-a-large-cup method [37–39]. Through these assessments, material properties of suspensions were derived, including the particle size distribution, compressive yield stress, $P_y(\phi)$, hindered settling function, $R(\phi)$, and shear yield stress, $\tau_y(\phi)$. Using $P_y(\phi)$ and $R(\phi)$, filtration performance was predicted using a fixed cavity filter press model [40].

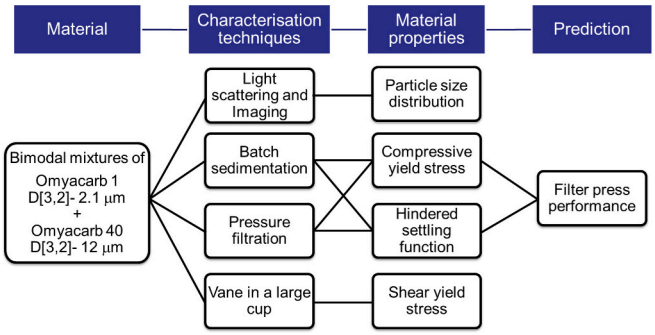

Fig. 1. Overview of characterisation techniques, experimental analysis and filter press performance prediction used in this work.

2.2. Bimodal calcium carbonate suspensions

Calcium carbonate was selected for its consistent self-coagulation and reproducible particle size across different batches. The objective was to replicate various bimodal mixtures using ultra-fine particles with uniform coagulation states and consistent surface interactions. The study aimed to illustrate a method for comparing dewaterability based solely on variations in particle size distribution.

A pycnometer cup was used to measure the densities of different suspensions. The densities of calcium carbonate and Milli-Q water used in the calculations were 2700 kg/m^3 and 998 kg/m^3, respectively. All suspensions were prepared at a solids volume fraction, ϕ, of 0.30 v/v with a background electrolyte concentration of 0.01 M KNO_3 [2,41]. The suspensions were gently mixed for 24 h using an overhead stirrer to ensure homogeneity. Consistency across repeated experiments using fresh batches further validated this approach.

For solids concentration measurement, dissolved solids in the liquor (post-vacuum filtration) and the dry mass fraction, including dissolved solids, were determined by oven-drying liquor and suspension at 105 °C for 24 h. The pH of all calcium carbonate suspensions was measured to be 8.4 ± 0.1. No pH adjustment was made, as calcium carbonate naturally buffers to this pH, which corresponds to its isoelectric point. This pH ensured cohesive or aggregated particles due to Van der Waals attraction, capturing the actual particle size distribution rather than dispersing or breaking the aggregates. The study maintained constant surface interaction conditions. Alteration of surface interaction through salt addition and pH changes would constitute a separate study [35], and each new surface interaction condition potentially impacts permeability, compressibility, and shear rheology differently. However, the method being presented in this study for comparing dewaterability between samples would remain consistent, regardless of variations in surface interaction conditions.

2.3. Particle size distribution and microscopic images

The particle size distributions (PSD) were measured using the Malvern Mastersizer 3000. The PSD of mixtures containing ultra-fine and coarser calcium carbonate are depicted in Fig. 2, with X representing the fraction of coarser calcium carbonate. The Sauter mean diameters, D[3,2], of the calcium carbonates Omyacarb 1 and Omyacarb 40 were determined to be 2.1 μm and 12.2 μm (Table 1), respectively. A stirrer speed of 2600 rpm was employed to prevent particle settling. Fig. 2 outlines the volumetric size distribution of the coarser calcium carbonate, ranging from $d_{10} = 5.13$ μm to $d_{90} = 116$ μm, indicating the presence of fine particles as well. Conversely, the ultra-fine calcium carbonate exhibited a narrower size distribution, with $d_{10} = 1.06$ μm to $d_{90} = 6.16$ μm. In the realm of mineral processing, particles smaller than 100 μm are classified as “fines”, while those smaller than 5 μm are termed “ultra-fines” [42]. Given the range of particle sizes in both calcium carbonates and using d_{90} values, all the particles in this work are

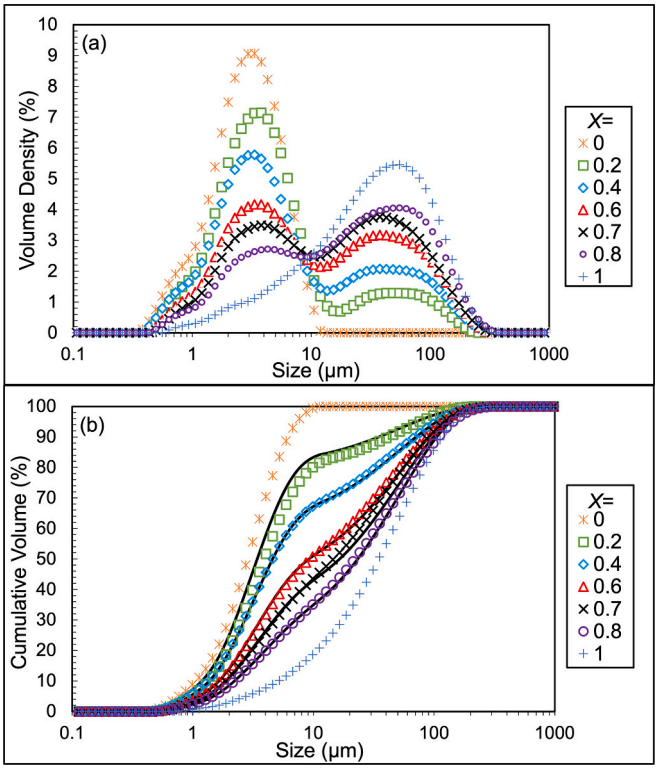

Fig. 2. (a) Frequency and (b) Cumulative particle size distributions of bimodal calcium carbonate mixtures where X is the fraction of coarser calcium carbonate. In (b), the lines for the mixtures are linear combinations of the pure ultra-fine and coarser particles, whereas the data points are the actual data from the Mastersizer.

Table 1
Summary of light scattering particle size distribution results of ultra-fine and coarser calcium carbonate mixtures. The specific surface area is calculated from the light scattering results and solids density.

	Mass fraction of coarser calcium carbonate, X						
	0	0.2	0.4	0.6	0.7	0.8	1
D [3,2] (μm)	2.13	2.52	3.13	4.35	5.21	6.28	12.2
D [4,3] (μm)	3.29	8.02	21.4	29.4	32.4	40.9	49.4
d_{10} (μm)	1.06	1.19	1.33	1.68	1.91	2.22	5.13
d_{50} (μm)	2.85	3.33	4.58	9.38	14.7	22.0	34.7
d_{90} (μm)	6.16	19.8	68.8	86.0	88.9	109	116
Specific Surface Area (m^2/kg)	2823	2383	1919	1379	1152	955.3	490.8

fines or ultra-fines. However, for clarity during discussion, Omyacarb 1 is referred to as the ultra-fine particle and Omyacarb 40 as the coarser particle.

In Fig. 2(b), the black lines representing the mixtures of coarser and ultra-fine particles are linear combinations of the distributions for the pure materials. The close agreement with experimental data confirms minimal errors in mixing the stock suspensions, ensuring no segregation or artifacts in light scattering due to polydispersity.

Table 1 presents two types of mean diameters: the Sauter mean diameter, D [3,2], which represents the diameter of a sphere that has the same volume-to-surface area ratio as the entire particle sample (Eq. (1)), and the de Brouckere mean diameter, D [4,3], which is the volume-weighted mean diameter of the particles (Eq. (2)) [43].

$$D[3,2] = \frac{\sum n_i D_i^3}{\sum n_i D_i^2} \tag{1}$$

$$D[4,3] = \frac{\sum n_i D_i^4}{\sum n_i D_i^3} \tag{2}$$

D [4,3] was measured at 3.29 μm and 49.4 μm for the ultra-fine and coarser calcium carbonate, respectively. Analysis later in this work was based on D [3,2], which is related to surface area, rather than D [4,3], which is related to volume, as particle surface area typically governs rheology and solid-liquid separation. The specific surface area of the coarser calcium carbonate was determined to be 490.8 m^2/kg, which nearly doubles to 955.3 m^2/kg with the addition of 20 % ultra-fines (Table 1). This increase in surface area due to a small addition of ultra-fines is expected to impact dewatering properties significantly. The increase from 0 to 20 % is proportionally almost as much as transitioning from 20 % to 100 % ultra-fines suspension, which results in a further 2.96 times increase in specific surface area, reaching 2823 m^2/kg. Note that these values of surface area were calculated from the particle size distribution and may underestimate the actual external surface area due to coagulation by Van der Waals forces [24].

The shape of the calcium carbonate powders was investigated using a scanning electron microscope (SEM) (Hitachi FlexSEM 1000), as depicted in Fig. 3. SEM imaging showed non-spherical angular particles typical of a crushing or grinding process. The particle sizes in the images correlate with the particle size distributions, illustrating a diverse range of particle sizes spanning from 1 to 250 μm for the coarser calcium carbonate (Omyacarb 40). At the same time, the ultra-fine sample (Omyacarb 1) exhibited a very narrow range of particle sizes.

2.4. Compressional rheology

2.4.1. Stepped pressure filtration

The compressibility and permeability of suspensions at high solids volume fractions were determined using a stepped pressure filtration method [38,44]. The experiments were conducted at six different pressures: 20 kPa, 40 kPa, 80 kPa, 150 kPa, 300 kPa, and 600 kPa, employing a 0.22 μm PVDF (polyvinylidene fluoride) membrane (Durapore, Merck).

In the compressibility tests, after the final pressure was applied, the solids volume fraction of the cake was measured using oven drying at 105 °C for 24 h. Subsequently, the volume fractions at all preceding pressures were calculated from this data to determine $P_y(\phi)$.

For the permeability tests, the parameter $R(\phi)$ was derived from the filtration data using Eq. (3), where β^2 represents the slope of t vs V^2 in a constant pressure filtration experiment (where t stands for time and V denotes the filtrate volume).

$$R(\phi) = \frac{2}{\frac{d\beta^2}{dP}} \left(\frac{1}{\phi_0} - \frac{1}{\phi}\right)^2 (1-\phi)^2 \tag{3}$$

2.4.2. Batch sedimentation

Transient batch sedimentation assessed the compressibility and permeability at low solids volume fractions. Suspensions were prepared below their gel point and settled in flat-bottom measuring cylinders with 0.5 L measuring cylinders with an internal diameter of 0.05 m. Before commencing the tests, the suspensions were homogenised using a hand-operated plunger. The height of the suspension-liquid interface was recorded over time until it remained constant for at least 50 % of the total experimental duration. The data were analysed utilising the approach outlined by Lester et al. [45].

2.4.3. Dewaterability functions

$R(\phi)$ and $P_y(\phi)$ were determined at low solids concentrations from the batch sedimentation data using a modification of the Kynch method [45,46] and combined with the results obtained from filtration tests conducted at high solids volume fractions to give continuous functions for $R(\phi)$ and $P_y(\phi)$ spanning a wide range of solids volume fractions. The

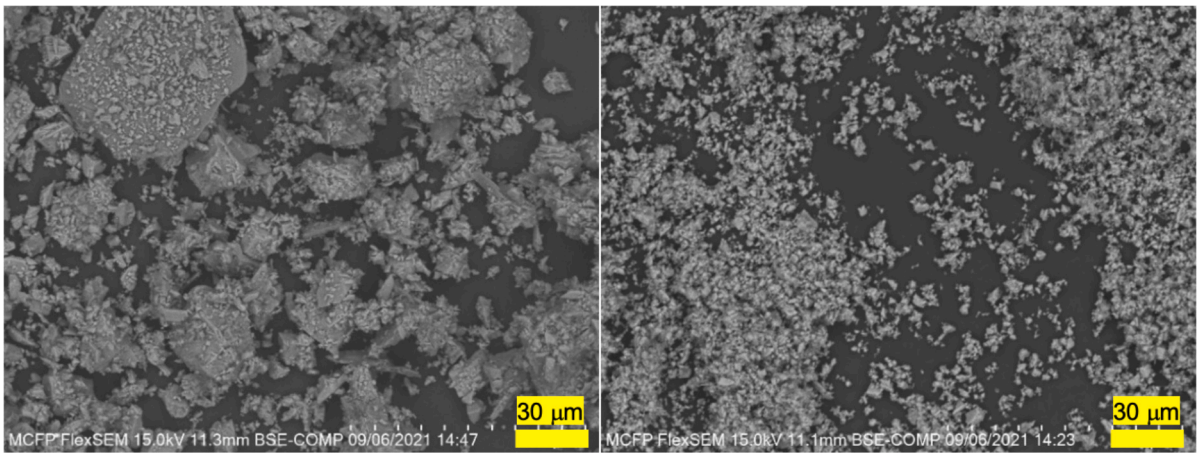

Fig. 3. SEM images of coarser (left) and ultra-fine (right) calcium carbonate particles.

dataset was fitted with empirical constitutive equations detailed in Eq. (4) [47]. These equations were selected for their high flexibility, enabling accurate representation of both low and high volume fractions across various materials. $R(\phi)$ was fitted using interpolating function.

$$P_y(\phi) = \begin{cases} 0 \text{ for } \phi < \phi_g \\ P_{y1}(\phi) = \left(\dfrac{a_1(\phi_{cp1}-\phi)(b_1+\phi-\phi_{g1})}{\phi-\phi_{g1}}\right)^{-k_1} \text{ for } \phi_g < \phi_p \\ P_{y2}(\phi) = \left(\dfrac{a_2(\phi_{cp2}-\phi)(b_2+\phi-\phi_{g2})}{\phi-\phi_{g2}}\right)^{-k_2} \text{ for } \phi_p < \phi_{cp} \end{cases} \tag{4}$$

ϕ_{cp} is the solids volume fraction at close packing and $a_1, a_2, b_1, b_2, \phi_{g1}, \phi_{g2}, \phi_p, \phi_{cp1}, \phi_{cp2}, k_1, k_2, r_a, r_b, r_g$, and r_n are parameters obtained through the fitting of experimental data.

2.5. Shear yield stress

The shear yield stress was determined using the vane-in-a-cup method by Nguyen and Boger [48]. In this technique, a four-bladed vane was submerged into the suspension and rotated at a controlled speed of 0.2 rpm to ascertain the maximum torque, denoted as T_{max}. The torque was then converted into shear yield stress, represented as τ_y, employing the equation:

$$\tau_y = \frac{T_{max}}{K} \tag{5}$$

Here, the vane constant, K, is contingent upon the dimensions of the vane as shown in Eq. (6). H_v and D_v correspond to the height (30.13 mm) and diameter (9.98 mm) of the vane, respectively.

$$K = \frac{\pi D_v^3}{2}\left(\frac{H_v}{D_v}+\frac{1}{3}\right) \tag{6}$$

To minimise wall effects, the vane was positioned within a cup with a diameter six and a half times that of the four-bladed vane [39,49]. Before each yield stress measurement, the suspension was thoroughly mixed for 2 min using an overhead stirrer rotating at approximately 200 rpm. Additionally, the cup was gently tapped on the bench for 30 s to facilitate the escape of any entrapped air bubbles. Afterwards, the vane was fully submerged in the suspension. After a 2-min waiting period, the vane was set in motion at 0.2 rpm, and torque was recorded over time. The shear yield stress was determined from the peak torque. Each measurement was repeated until the variation in shear stress was within 10 %.

2.6. Filter press modelling

A numerical model developed by Stickland et al. [40] for a fixed cavity filter press, which uses the theoretical framework of Buscall and White [17] and the constant pressure piston-driven filtration model of Landman and White [18], was used to compare the filtration process performance of the different particle mixtures. The model simplifies the filtration separation process into one dimension, and the gravitational forces are assumed to be negligible. Key inputs for the model include material properties ($P_y(\phi)$, $R(\phi)$, and ϕ_0), cavity width (equal to $2h_0$), membrane resistance R_m, handling time t_H, loading time t_L, and filtration pressure ΔP, allowing for the calculation of solids volume fraction distribution and specific volume of filtrate, $V(t_F)$, over filtration time, t_F [40].

The average suspension throughput per unit membrane area, Q, is determined by Eq. (7) where t_L is part of t_F. The average cake concentration, ϕ_F, is expressed in Eq. (8).

$$Q = \frac{V(t_F)+h_0}{t_F+t_H} \tag{7}$$

$$\phi_F = \phi_0\left(1+\frac{V(t_F)}{h_0}\right) \tag{8}$$

For the model predictions in this work, the cavity width (twice the initial height, h_0) was set at 3 cm, while the initial concentration, ϕ_0, was 0.10 v/v. Membrane resistance, R_m, was considered negligible compared to filter cake resistance. The handling time, t_H, for each filter press run was assumed to be 300 s, and the loading time, t_L, was 0. Additionally, the filter was operated under a constant fill pressure, ΔP, of 600 kPa.

3. Results and discussion

3.1. Material characterisation

3.1.1. Compressive yield stress

In the context of increasing concentrations of ultra-fine particles within suspensions, the behaviour of compressive yield stress exhibits complex dynamics. As ultra-fine particles contribute significantly to the surface area, increasing the number of particle-particle interactions, the compressive yield stress tends to rise. Conversely, when ultra-fine particles are present in modest quantities, they are expected to enter the interstitial spaces between the coarser particles and reduce the compressive yield stress. The expectation is an optimum packing configuration, resulting in the lowest compressive yield stress. Beyond this optimum packing, the inability of ultra-fine particles to fit into the interstices is expected to lead to a subsequent increase in compressive

yield stress.

In our investigation, various mixtures of calcium carbonate spanning the range from $X = 0$ to 1.0 were subjected to batch sedimentation and stepped pressure filtration methods. Through these experiments, the compressive yield stress curves across a wide spectrum of solids volume fractions were obtained using Eq. (4) (Fig. 4).

The $X = 1.0$ suspension has a higher gel point and is closer to the random close packing fraction, making it more incompressible and easier to dewater than $X = 0$ suspension. When comparing $X = 1.0$ and 0, the suspension with the ultra-fine particles exhibits significantly higher compressive yield stress for any given solids volume. This difference can be attributed to the reduced surface area of coarser particles leading to diminishing interparticle interactions and allowing for more efficient particle packing. Consequently, for a given compressive load ($P_y(\phi)$), suspensions with coarser particles ($X = 1.0$) demonstrate superior equilibrium dewatering capabilities, achieving substantially higher solids volume fractions at long times than those rich in ultra-fine particles ($X = 0$).

For instance, under a compressive load of 600 kPa, the coarser particle mixture can ultimately attain a solids volume fraction of 63.1 v/v%, whereas the ultra-fine particle mixture achieves only 52.9 v/v%, a notable 10.2 v/v% difference in moisture content despite identical pressure conditions. Similarly, at 20 kPa compressive load, the moisture content differential amounts to 16.5 v/v%. The transition from coarser calcium carbonate particles, characterised by a D [3,2] of 12.2 μm to ultra-fine suspensions featuring a D [3,2] of 2.1 μm - a sixfold reduction in size - profoundly influences the equilibrium extent of dewatering. This substantial reduction in particle size underscores a significant challenge in achieving low moisture levels, particularly in industrial applications with ultra-fine particles. Current state-of-the-art technologies may struggle to meet the stringent moisture level targets in such applications unless higher pressures are utilised.

Bimodal mixtures comprising ultra-fine and coarser particles exhibit reduced equilibrium solids volume fractions at given pressures compared to $X = 1.0$ mixture. However, beyond certain pressure thresholds, suspensions with $X = 0.8$, 0.7, and 0.6 achieve higher solids concentrations than the pure coarser suspension. The pressure thresholds for achieving this enhancement are 64 kPa, 131 kPa, and 531 kPa for $X = 0.8$, 0.7, and 0.6, respectively. Above these specific pressures, it is reasonable to infer that the ultra-fine particles are forced into the interstitial gaps of coarser particles, enhancing packing efficiency. The lower the amount of ultra-fine particles present, the lower the pressure required to give better packing than the $X = 1.0$ suspension. The highest solids volume fraction was obtained at 69.0 v/v% at just 300 kPa of pressure when the proportion of ultra-fine present was 20 % ($X = 0.8$). The results demonstrate that both surface area and particle packing affect compressibility, with surface area dominating for particles less than about 10 μm.

The gel point (ϕ_g), presented in Fig. 5, marks the point where $P_y(\phi)$ equals zero. Suspensions containing ultra-fine particles exhibit a lower gel point of 0.22 v/v, indicative of a more expansive interparticle network, in contrast to coarser particle suspensions registering a gel point of 0.38 v/v.

With the gradual increase in the proportion of ultra-fine particles within mixtures, some of these particles fill the interstices among coarser particles, facilitating the formation of a continuous structure. This filling also reduces the proportion of isolated coarser particles, lowering the gel point. The values for $X = 0.2$ and 0.8 deviate from the trend, and when excluded, the gel point shows a linear relationship with X, achieving an R^2 of 0.99, as shown in Fig. 5. The slight increase in gel point from $X = 1.0$ to 0.8 aligns with the findings of Lim et al. [28], who similarly observed a peak in the gel point with minimal addition of fines to a coarse sand (D [4,3] = 1.1 mm) suspension, followed by a subsequent decrease with X less than 0.8. This result suggests that packing geometry plays a crucial role in the gel point. At high X, coarser particles form a network at their gel point, with ultra-fine particles filling the voids, collectively increasing the overall gel point [28]. However, when $X = 0.2$, the gel point decreases slightly compared to 100 % ultra-fines ($X = 0$), underscoring the influence of packing constraints over interparticle interactions in this scenario.

3.1.2. *Hindered settling function*

An increase in ultra-fine particles within a suspension is anticipated to cause a decrease in permeability throughout the entire solids volume fraction range due to increased fluid drag from increased specific surface area, impeding their efficiency in dewatering processes. Enhanced permeability plays a pivotal role in dewatering applications, facilitating expedited throughput and diminishing the need for larger equipment, thus mitigating capital costs. Consequently, understanding the extent of permeability differences between suspensions assumes paramount significance and the methodology elucidated in this study offers valuable insights.

Fig. 6 presents the hindered settling functions for calcium carbonate mixtures spanning from $X = 0$ to 1.0. As with the compressive yield stress results, data points corresponding to higher solids content originate from filtration tests, while those for lower solids content stem from sedimentation tests.

The hindered settling function is inversely related to permeability [50]. As the proportion of ultra-fine particles increases within the

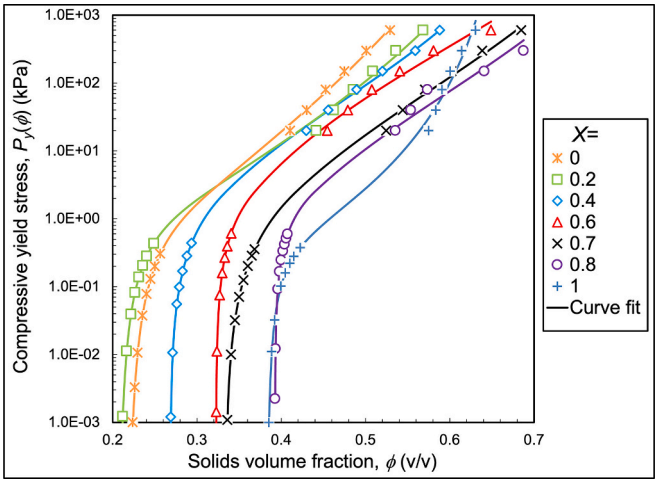

Fig. 4. Compressive yield stress variation with solids volume fraction for different calcium carbonate mixtures and fitted using Eq. (4). X is the fraction of coarser calcium carbonate.

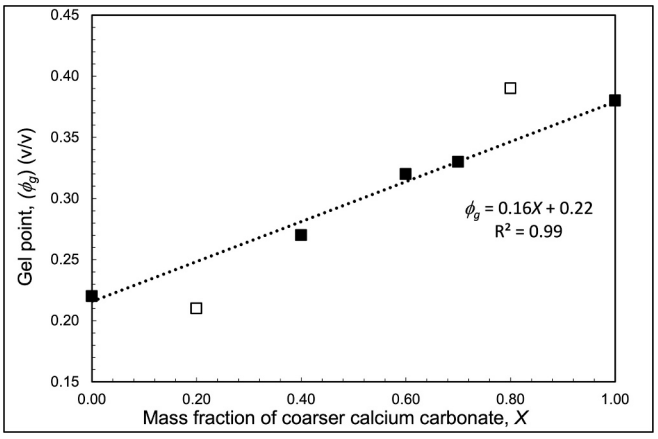

Fig. 5. Gel points of various calcium carbonate mixtures plotted as a function of the fraction of coarser particles and fitted using a linear regression ignoring the open symbols.

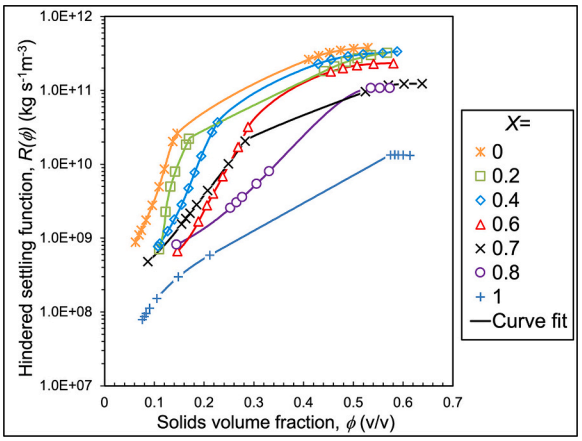

Fig. 6. Hindered settling function variation with solids volume fraction for different calcium carbonate mixtures. X is the fraction of coarser calcium carbonate.

mixture, these smaller particles increase drag resistance for a given solids volume fraction, consequently diminishing permeability. Notably, suspensions comprising coarser particles ($X = 1.0$) demonstrate hindered settling rates at least an order of magnitude lower than those composed of ultra-fine particles ($X = 0$) across the entire spectrum of solids volume fraction. For instance, at 52 v/v%, the coarser suspension gives a permeability approximately 40 times higher than the ultra-fine suspension, indicating substantially faster dewatering processes and expected improvements in throughput.

Introducing 20 % ultra-fines ($X = 0.8$) results in a notable increase in the hindered settling function, associated with an expected decline in the dewatering rate. For instance, at 57.5 v/v%, the permeability decreases by around eight times. This underscores a discernible trend wherein permeability diminishes with an increased proportion of ultra-fines in the mixture and that only a small amount of ultra-fines can have a significant effect.

However, intriguing discrepancies emerge, particularly around higher solids volume fractions for mixtures comprising 80 % and 60 % ultra-fines ($X = 0.2$, 0.4). These inconsistencies hint at a nuanced scenario where permeability slightly improves at higher concentrations, notably when the suspension contains 80 % ultra-fines compared to 60 %. Similarly, at lower solids volume fractions, the suspension featuring 40 % ultra-fines exhibits superior permeability compared to its 30 % ultra-fines counterpart.

In theory, increasing the surface area per unit volume—such as by increasing the fraction of ultra-fine particles—should reduce permeability due to enhanced particle packing and reduced pore space. However, the observed slight improvement in permeability at 80 % and 40 % ultra-fines suggests that additional effects may be influencing the system. One possible explanation is that at high ultra-fine concentrations, the fine particles may layer onto the surfaces of the larger particles, effectively smoothing the pore network and reducing tortuosity. According to the Carman-Kozeny equation, permeability is strongly affected by both porosity and tortuosity. If ultra-fines form a more structured arrangement around coarser particles, the resulting flow paths may become less convoluted, leading to a slight increase in permeability. These findings highlight the intricate relationship between particle composition and permeability dynamics in the studied mixtures.

Additional batches of suspensions were meticulously prepared, and the stepped pressure filtration procedure was replicated. The suspensions encompassed various compositions, including $X = 1.0$, 0.8, 0.2, and 0. The consistency observed in both compressive yield stress and hindered settling function across these repeat experiments suggests that the tests are reproducible and unaffected by any degradation phenomena of either coarser or ultra-fine calcium carbonate particles.

3.1.3. Shear yield stress

The influence of ultra-fine particles on shear yield stress is a critical aspect to consider in understanding the rheological behaviour of suspensions. This relationship between shear yield stress and ultra-fine content was investigated across various calcium carbonate mixture concentrations, with results shown in Fig. 7. The data for each suspension was fitted using an exponential fit, which generally fitted the data better than a power-law fit. However, shear yield stress measurements were capped at 1000 Pa due to limitations arising from sample fracturing and the fitted exponential functions should not be extrapolated in either direction since the shear yield stress will be negligible below the gel point and asymptote to infinity at close packing.

The dependence of shear yield stress on both volume fraction and particle size is evident. As volume fraction increases and particle size decreases, shear yield stress has a corresponding increase. This phenomenon is attributed to the increased surface area in ultra-fine particle suspensions, resulting in greater density of inter-particle interactions and higher resistance to yield compared to coarser particle suspensions. For instance, at a concentration of 46 v/v%, the shear yield stress of ultra-fine particle suspensions surpasses that of coarser particle suspensions by more than two orders of magnitude, signifying a substantial difference with implications for processing and transport applications. Overall, the observed trend underscores the direct relationship between shear yield stress and the proportion of ultra-fines in the suspension.

Furthermore, to validate the consistency of experimental findings, multiple fresh batches of select suspensions ($X = 1.0$, 0.8, and 0) were prepared and subjected to repeated experiments. The results demonstrated a small variance within a 10 % margin, indicating minimal preparation artifacts. Additionally, measurements of shear yield stress for the ultra-fine calcium carbonate suspensions were conducted over 28 days using the same sample, revealing consistent outcomes without measurable aging or dissolution effects. The results presented in Fig. 7 were fitted using the expression:

$$\tau_y = ae^{b\phi} \tag{9}$$

a and b represent fitting parameters. Fig. 8 illustrates a clear dependency of both coefficients a and b on the Sauter mean diameter (d_s) of the mixture, governed by the following trends:

$$a = 6.91 d_s^{-4.92} \tag{10}$$

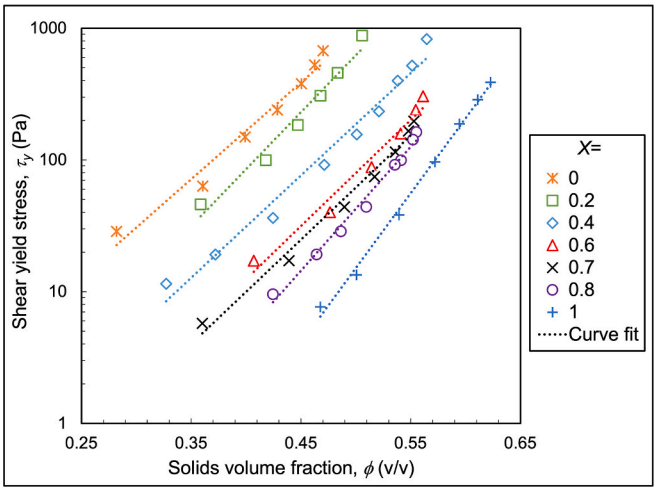

Fig. 7. Shear yield stress from peak stress upon flow start-up as a function of solids volume fraction for different calcium carbonate mixtures and fitted using an exponential fit (Eq. (9)). X is the fraction of coarser calcium carbonate.

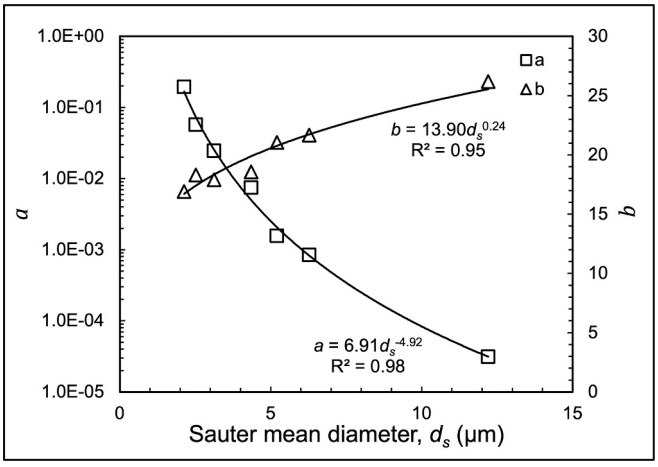

Fig. 8. Variation of shear yield stress scaling parameters, *a* and *b,* with Sauter mean diameter for different calcium carbonate mixtures.

$$b = 13.90d_s^{0.24} \tag{11}$$

Substituting Eqs. (10) and (11) into Eq. (9) yields a comprehensive model for predicting the shear yield stress of the investigated calcium carbonate bimodal mixtures:

$$\ln(\tau_y) = \ln(d_s^{-4.91}) + 13.90d_s^{0.24}\phi + 1.93 \tag{12}$$

This equation enables the prediction of shear yield stress for calcium carbonate mixtures based on known d_s values across a range of solid volume fractions (ϕ). It is crucial to note that this prediction applies solely to the selected calcium carbonate sizes with the same suspension conditions (pH, ionic strength) used in this study. Nevertheless, this methodology holds promise for extension to any suspensions containing different-sized particles.

Several studies by different researchers have demonstrated that when surface chemistry remains consistent, the shear yield stress exhibits an inverse relationship with the square of particle size at a given solids volume fraction [35,51,52]. The behaviour depicted in Fig. 9 somewhat aligns with this finding, albeit with a nuanced observation: the 100 % and 80 % ultra-fines mixtures ($X = 0$ and 0.2) deviate from the expected scaling behaviour, necessitating a particle size descriptor slightly smaller than d_s to achieve the anticipated scaling behaviour. In Fig. 2(a), $X = 0$ and 0.2 exhibit primarily monomodal and slightly bimodal distributions compared to other suspensions. This implies a potential bimodal threshold where packing considerations dominate surface area changes, or it could be attributed to ultra-fine particles aggregating more at the smaller end of the particle size distribution, thereby resulting in higher d_s values.

3.1.4. Comparison of compressive and shear yield stress

The ratio of shear yield stress to compressive yield stress $\tau_y/P_y(\phi)$, is depicted in Fig. 10, showcasing a range spanning from 0.03 at low volume fractions to 0.001 at higher volume fractions, consistent with findings in prior research [35,52–55]. This ratio has significant implications for dewatering since the strength in shear is much less than in compression and is vital for understanding multidimensional suspension mechanics problems such as wall adhesion in batch sedimentation [56]. In filtration applications, integrating shear will enhance dewatering efficiency, as indicated by previous studies [41,57–61].

The failure mode is expected to differ between shear and compressional deformation and the mechanistic contributions to failure are expected to vary as a function of solids concentration [62]. In pure shear, suspensions first strain harden, then show shear rate-dependent strain softening before yielding and flowing [63]. From the gel point to solids concentrations around 30 v/v%, the dominant failure mechanism is bond breakage at strains in the order of 0.001 to 0.01. At higher concentrations, the particles form a steric cage that undergoes 'cage melting' at strains *circa* 1 [64]. Mechanistic examination of the mode of failure in compression is not as detailed but is expected to be simply strain hardening and then cage melting at a rate determined by the permeability as the suspension consolidates [62]. The difference in the shear-to-compressive yield stress ratio is expected to be associated with the benefit of the extra degrees of freedom that allow strain softening in sheared systems. A minimum point in the shear-to-compressive yield stress ratio was observed in all the suspensions except for the coarser calcium carbonate suspension. It is speculated here that this may represent a point where at least one degree of freedom in terms of failure is lost in the sheared system as steric hindrance increases. This minimum appears to be affected by the bimodal nature of the mixtures, given that $X = 0.4$ and $X = 0.6$ have the lowest shear-to-compressive yield ratio.

3.2. Filter press modelling

3.2.1. Solids throughput

The dewaterability characterisation reveals significant variations in the magnitude of $P_y(\phi)$ and $R(\phi)$ across the range of solid concentrations under investigation. Since both parameters influence dewatering efficiency, it remains challenging to understand, solely from these charac-

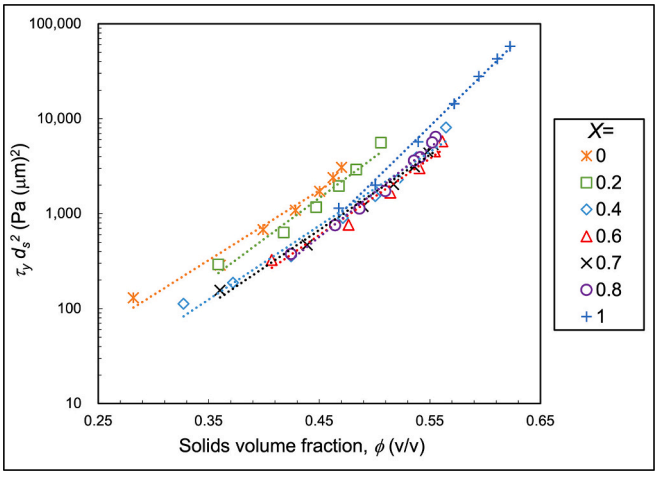

Fig. 9. Product of shear yield stress with d_s^2 as a function of solids volume fraction and fitted using an exponential fit (Eq. (9)). *X* is the proportion of coarser calcium carbonate.

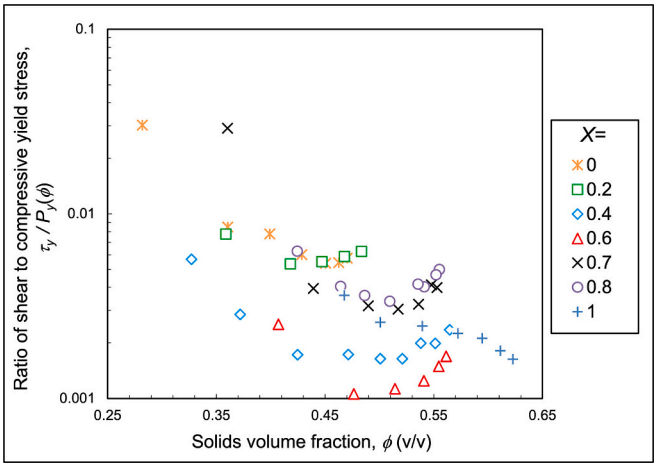

Fig. 10. Ratio of shear yield to the compressive yield stress variation with solids volume fraction for different calcium carbonate mixtures. *X* is the proportion of coarser calcium carbonate.

terisations, which suspension demonstrates superior dewaterability or, the scalar difference between the coarser and ultra-fine particle combinations. Instead, $P_y(\phi)$ and $R(\phi)$ serve as crucial inputs for process modelling, such as the validated filter press model employed in this study [65], although alternative processes such as thickening, centrifugation, or other filter configurations could have been considered.

This approach quantitatively compares material property differences among suspensions under consistent geometric, feed, and pressure conditions. The model offers flexibility to explore various parameters, such as adjusting the feed solids concentration or the cavity width [65], providing a versatile framework for comprehensive analysis study. This study selected a single pressure condition of 600 kPa based on the maximum reliable pressure used in the material characterisation.

Utilising the parameters $\phi_0 = 0.10$ v/v, $t_H = 300$ s, $t_L = 0$, cavity width = 3 cm, and negligible R_m, the relationship between the average specific solids throughput, $\phi_0 Q$, and the average cake solids, ϕ_F, was calculated, as demonstrated in Fig. 11. The specific solids throughput exhibits an initial increase, reaching a peak value, beyond which it diminishes with increasing cake solids concentration. As a rule of thumb, the maximum throughput occurs when the filtration time constitutes half of the total duration for each run [66].

Initially, at low cake solids concentrations, all suspensions exhibit comparable throughputs, owing to the insignificance of filtration time relative to the filter handling time. However, at higher cake concentrations, the presence of ultra-fine particles begins to influence throughput, along with the maximum achievable filtration extent at 600 kPa. For instance, to attain a cake solids concentration of 50 v/v%, the solids throughput of a suspension containing 20 % ultra-fines ($X = 0.8$) and a suspension containing 100 % ultra-fines ($X = 0$) diminishes by approximately 1.6 times and 2.4 times, respectively, when compared to a coarser suspension ($X = 1.0$).

When the proportion of ultra-fines exceeds or equals 40 % ($X \leq 0.6$), the model indicates that solids throughput is primarily dictated by the ultra-fine component, with marginal variations in compressibility. This highlights the advantages of segregating coarser and ultra-fine components in a filtration feed, particularly if the coarser fraction could be dewatered using less capital-intensive and operationally less costly dewatering equipment.

3.2.2. Filtration area and time requirements

The model results are used to calculate the necessary filtration time and area for achieving desired levels of solids throughput and filter cake solids concentration. As an illustration, to process solids at a throughput of 100 t per hour, with a final cake concentration (ϕ_F) of 0.5 v/v, based on a solids density of 2700 kg/m^3, we conducted predictions for the requisite filtration area and time for a filter press. An initial concentration (ϕ_0) of 0.10 v/v was used for the analysis.

To attain the desired throughput and cake concentration, the filtration time for the coarser calcium carbonate suspension (with a D [3,2] of 12.2 μm) is predicted to be 31 s. Conversely, the ultra-fine calcium carbonate suspension (with a D [3,2] of 2.1 μm) necessitates 505 s, marking an approximately 16-fold difference. In terms of required filtration area, the coarser suspension demands 452 m^2, while the ultra-fine suspension calls for 1100 m^2, reflecting an increase of approximately 2.4 times. The largest filter press, the GHT5000F Domino, has a filtration area of 2850 m^2 [67]. Based on the parameters used in the model, this press could process 6219 t/d with the ultra-fine suspension, whereas it could handle 15,120 t/d with the coarser suspension.

Further analysis indicates that suspensions containing 0 to 60 % ultra-fines (with D [3,2] ranging from 12.2 to 4.4 μm) exhibit an increase in both area and time requirements as the ultra-fine content rises. Notably, at ultra-fine contents ≥60 %, both the area and time requirements resemble those of a 100 % ultra-fine suspension, indicating minimal further change in behaviour. This trend is attributed to the relatively small variations in the Sauter mean diameter across suspensions with ultra-fine contents in this range, even though the diameter changes systematically.

The filtration time and area were plotted against the Sauter mean diameter, as shown in Fig. 12. We would expect a $1/d_s^2$ relationship based on the Carman-Kozeny equation. However, the model data indicated that the filtration time decreases exponentially with increasing Sauter mean diameter, d_s (in μm), according to the equation:

$$t_F = 1142\exp(-0.28 d_s) \tag{13}$$

This exponential model provided a better fit to the data. Meanwhile, the filtration area, A, is a linear function of t_F, given by:

$$A = 1.37(t_F + 300) \tag{14}$$

Note that the total cycle time and thus the required filtration area for $X = 1$ is dominated by the handling time of 300 s compared to the filtration time of 31 s, whereas the filtration time is similar or greater than the handling time for all the other results. Although assuming a constant handling time of 300 s per batch standardises the analysis, it highlights the challenge inherent to maximising filter area utilisation in filter presses due to their fixed cavity width and batch nature. Adjustments, such as employing thicker cavities, could address this issue, but this would reduce the adaptability of the system to suspensions with

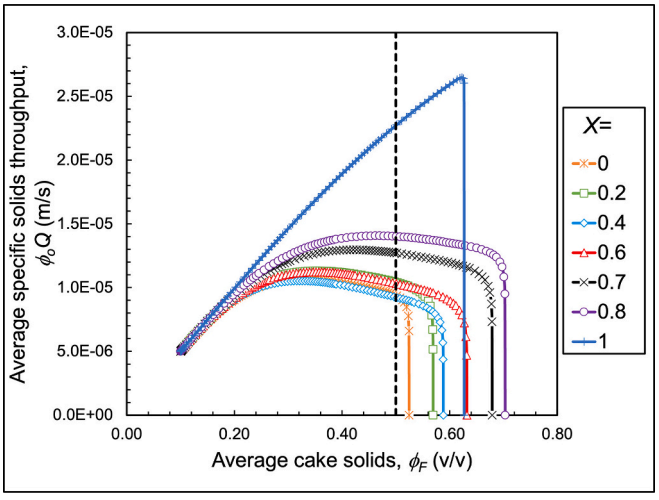

Fig. 11. Solids throughput predictions for different calcium carbonate suspensions using the filter press model. X is the proportion of coarser calcium carbonate and $\phi_F = 0.5$ v/v is the comparison point.

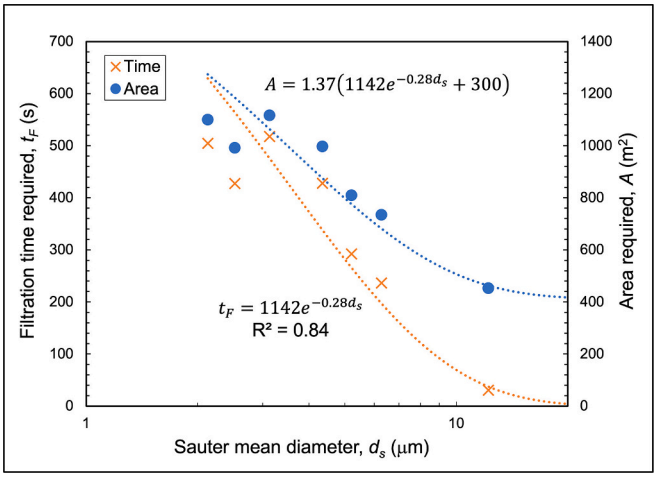

Fig. 12. Filter press area and filtration time required as a function of Sauter mean diameter. Each point represents 100 tonnes per hour solids throughput of calcium carbonate suspensions at $\phi_0 = 0.1$ v/v to reach $\phi_F = 0.5$ v/v.

varying particle sizes.

3.3. Conclusions

Two different sizes of calcium carbonate particles, with Sauter mean diameters of 2.1 μm and 12.2 μm, were used to represent ultra-fine ($X = 0$) and coarser-sized ($X = 1$) suspensions, respectively. By systematically adding ultra-fine particles and using minimal samples, it is possible to represent a variety of particulate systems (in terms of particle size rather than mineralogy), enabling quantification of the impact of adding ultra-fine particles to particle mixtures without altering the surface chemistry. The study underscores the significant particle size dependency of dewatering, where the particle systems comprising the model mixtures are in a similar state of coagulation.

The study delves into how samples of varying particle sizes can be assessed regarding dewatering extent and rate, revealing how filtration conditions can become constraining with increased ultra-fine particle proportions. Under a compressive load of 600 kPa, the $X = 0$ suspension, with a D [3,2] six times lower than the $X = 1$ suspension, resulted in a cake with 10.2 v/v% higher moisture content, highlighting the difficulty in dewatering ultra-fine particles. However, beyond 64 kPa of compressive load, the blend containing 20 % ultra-fines ($X = 0.8$) exhibited superior packing compared to the $X = 1$ suspension, capitalising on smaller particles filling void spaces among coarser ones. Similarly, $X = 0.7$ and 0.6 achieved higher solids concentrations at equilibrium above 131 kPa and 531 kPa, respectively, indicating optimum packing arrangements when the proportion of ultra-fines and coarser particles is balanced, which can enhance the achievable dewatering extent. The gel point exhibited a linear decrease from $X = 1$ to $X = 0$ suspensions, with an R^2 value of 0.99, without $X = 0.8$ and 0.2, where these deviations occurred due to packing effects. In comparing the $X = 1$ and $X = 0$ suspensions, permeability decreased by at least one order of magnitude, while shear yield stress increased by up to two orders of magnitude.

To process 100 t/h of solids throughput, a numerical model of a fixed cavity filter press was employed to predict filtration time and thus calculate area requirements. This model enables a quantitative comparison of different samples and predicts the optimum solids throughput, filtration area and time necessary to attain specific final cake moisture levels, contingent upon the proportion of ultra-fine particles in suspensions.

To achieve a solids concentration of 0.5 v/v from an initial feed of 0.1 v/v using 600 kPa, the $X = 0$ suspension requires a filtration time 16 times longer than the $X = 1$ suspension. The filtration area needed was found to be 2.4 times greater than the $X = 0$ suspension, with the reduction in impact due to the role of handling time in batch filter operation. Dewatering exhibited high sensitivity to the level of ultra-fines in a mixture. As ultra-fines are added to the coarser suspension, the filtration time and required area increase dramatically until 60 % ultra-fines are reached, after which the requirements become similar to those of a 100 % ultra-fine suspension. The filtration time exhibits an exponential decrease with the Sauter mean diameter, whereas the filtration area is linearly dependent on the filtration time, to achieve a targeted final cake moisture content.

The shear yield stress of the suspensions was consistently two to three orders of magnitude lower than the compressive yield stress, irrespective of the fraction of ultra-fine particles present. Consequently, the findings indicate the potential for enhancing the dewatering process by incorporating shear into filtration devices alongside pressure application. Ongoing tests are exploring devices that can leverage this behaviour [41,68].

These findings have significant implications for dewatering various particulate systems with different material sizes. They are especially relevant in mineral tailings management, where tailings often exhibit heterogeneous particle size distributions.

CRediT authorship contribution statement

Sajid Hassan: Writing – review & editing, Writing – original draft, Visualization, Validation, Project administration, Methodology, Investigation, Formal analysis, Data curation. **Nilanka I.K. Ekanayake:** Writing – review & editing, Formal analysis. **Peter J. Scales:** Writing – review & editing, Supervision, Methodology, Funding acquisition, Conceptualization. **Robin J. Batterham:** Writing – review & editing, Supervision. **Anthony D. Stickland:** Writing – review & editing, Supervision, Software, Resources, Project administration, Methodology, Funding acquisition, Formal analysis, Data curation, Conceptualization.

Declaration of competing interest

The authors declare that they have no known competing financial interests or personal relationships that could have appeared to influence the work reported in this paper.

Acknowledgements

S Hassan is a recipient of the Research Training Program Scholarship from the University of Melbourne, and this project is funded by the Australian Research Council for the ARC Centre of Excellence for Enabling Eco-Efficient Beneficiation of Minerals, grant number CE200100009. The authors also thank Raul Cavalida for providing the SEM images and Dr. Mark Coghill from Rio Tinto for his valuable feedback on this paper.

Data availability

Data will be made available on request.

References

[1] M.L. Christensen, K. Keiding, Creep effects in activated sludge filter cakes, Powder Technol. 177 (1) (2007) 23–33.
[2] E. Höfgen, S. Kühne, U.A. Peuker, A.D. Stickland, A comparison of filtration characterisation devices for compressible suspensions using conventional filtration theory and compressional rheology, Powder Technol. 346 (2019) 49–56.
[3] B. Li, H. Zhang, K. Saranteas, M.A. Henson, A rigid body dynamics model to predict the combined effects of particle size and shape on pressure filtration, Sep. Purif. Technol. 278 (2021) 119462.
[4] S.S. Haramkar, G.N. Thombre, S.V. Jadhav, B.N. Thorat, The influence of particle (s) size, shape and distribution on cake filtration mechanics—a short review, C. R. Chim. 24 (2) (2021) 255–265.
[5] P. Bradu, A. Biswas, C. Nair, S. Sreevalsakumar, M. Patil, S. Kannampuzha, A. G. Mukherjee, U.R. Wanjari, K. Renu, B. Vellingiri, A.V. Gopalakrishnan, Recent advances in green technology and industrial revolution 4.0 for a sustainable future, Environ. Sci. Pollut. Res. 30 (60) (2023) 124488–124519.
[6] J.H. Hodgkinson, M.H. Smith, Climate change and sustainability as drivers for the next mining and metals boom: the need for climate-smart mining and recycling, Res. Policy 74 (2021) 101205.
[7] A.J. Whitworth, E. Forbes, I. Verster, V. Jokovic, B. Awatey, A. Parbhakar-Fox, Review on advances in mineral processing technologies suitable for critical metal recovery from mining and processing wastes, Clean. Eng. Technol. 7 (2022) 100451.
[8] R. Batterham, Trends in comminution driven by energy, Adv. Powder Technol. 22 (1) (2011) 138–140.
[9] C. Wang, D. Harbottle, Q. Liu, Z. Xu, Current state of fine mineral tailings treatment: a critical review on theory and practice, Miner. Eng. 58 (2014) 113–131.
[10] J.S. Adiansyah, M. Rosano, S. Vink, G. Keir, A framework for a sustainable approach to mine tailings management: disposal strategies, J. Clean. Prod. 108 (2015) 1050–1062.
[11] S. Palaniandy, M. Powell, Addressing water scarcity in mining through improved comminution practices, AusIMM Bull. 5 (2014) 50–52.
[12] J.R. Owen, D. Kemp, É. Lèbre, K. Svobodova, G. Pérez Murillo, Catastrophic tailings dam failures and disaster risk disclosure, Int. J. Disaster Risk Reduct. 42 (2020) 101361.
[13] K. Islam, S. Murakami, Global-scale impact analysis of mine tailings dam failures: 1915–2020, Glob. Environ. Chang. 70 (2021) 102361.
[14] H. Amar, M. Benzaazoua, A. Elghali, R. Hakkou, Y. Taha, Waste rock reprocessing to enhance the sustainability of phosphate reserves: a critical review, J. Clean. Prod. 381 (2022) 135151.
[15] B. Reichmann, J. Tomas, Expression behaviour of fine particle suspensions and the consolidated cake strength, Powder Technol. 121 (2) (2001) 182–189.

[16] H. Jones, D.V. Boger, Sustainability and waste management in the resource industries, Ind. Eng. Chem. Res. 51 (30) (2012) 10057–10065.
[17] R. Buscall, L.R. White, The consolidation of concentrated suspensions. Part 1.—The theory of sedimentation, J. Chem. Soc., Faraday Trans. 1: Phys. Chem. Condens. Phases 83 (3) (1987) 873–891.
[18] K.A. Landman, L.R. White, Solid/liquid separation of flocculated suspensions, Adv. Colloid Interf. Sci. 51 (1994) 175–246.
[19] S.J. Skinner, L.J. Studer, D.R. Dixon, P. Hillis, C.A. Rees, R.C. Wall, R.G. Cavalida, S.P. Usher, A.D. Stickland, P.J. Scales, Quantification of wastewater sludge dewatering, Water Res. 82 (2015) 2–13.
[20] R.J. Wakeman, M.N. Sabri, E.S. Tarleton, Factors affecting the formation and properties of wet compacts, Powder Technol. 65 (1) (1991) 283–292.
[21] J. Addai-Mensah, Enhanced flocculation and dewatering of clay mineral dispersions, Powder Technol. 179 (1) (2007) 73–78.
[22] C. Tien, Cake filtration research—a personal view, Powder Technol. 127 (1) (2002) 1–8.
[23] P.V. Lade, J.A. Yamamuro, C.D. Liggio, Effects of fines content on void ratio, compressibility, and static liquefaction of silty sand, Geomech. Eng. 1 (2009) 1–15.
[24] A. El-Husseiny, Improved packing model for functionally graded sand-fines mixtures—incorporation of fines cohesive packing behavior, Appl. Sci. 10 (2) (2020) 562.
[25] E. Löwer, F. Pfaff, T. Leißner, U.A. Peuker, Neighborhood relationships of widely distributed and irregularly shaped particles in partially dewatered filter cakes, Transp. Porous Media 138 (1) (2021) 201–224.
[26] F.M. Mahdi, T.N. Hunter, R.G. Holdich, A study of cake filtration parameters using the constant rate process, Processes 7 (10) (2019) 746.
[27] D.R. Dinger, J.E. Funk, Particle-packing phenomena and their application in materials processing, MRS Bull. 22 (12) (1997) 19–23.
[28] S. Lim, K.H. Ahn, S.J. Lee, A. Kumar, N. Duan, X. Sun, S.P. Usher, P.J. Scales, Yield and flow measurement of fine and coarse binary particulate mineral slurries, Int. J. Miner. Process. 119 (2013) 6–15.
[29] F.G.R. Gauthier, S.C. Danforth, Packing of bimodal mixtures of colloidal silica, J. Mater. Sci. 26 (22) (1991) 6035–6043.
[30] B.V. Velamakanni, F.F. Lange, Effect of Interparticle potentials and sedimentation on particle packing density of bimodal particle distributions during pressure filtration, J. Am. Ceram. Soc. 74 (1991) 166–172.
[31] P. Kaothon, S.-H. Lee, Y.-T. Choi, C.-Y. Yune, The effect of fines content on compressional behavior when using sand-kaolinite mixtures as embankment materials, Appl. Sci. 12 (12) (2022) 6050.
[32] Q.J. Zheng, R.Y. Yang, Q.H. Zeng, H.P. Zhu, K.J. Dong, A.B. Yu, Interparticle forces and their effects in particulate systems, Powder Technol. 436 (2024) 119445.
[33] T. Fedina, J. Sundqvist, A.F.H. Kaplan, The role of powder morphology in particle movement behavior in laser powder bed fusion with an emphasis on fluid drag, Powder Technol. 395 (2022) 720–731.
[34] U. Ulusoy, A review of particle shape effects on material properties for various engineering applications: from macro to nanoscale, Minerals 13 (1) (2023) 91.
[35] Z. Zhou, P.J. Scales, D.V. Boger, Chemical and physical control of the rheology of concentrated metal oxide suspensions, Chem. Eng. Sci. 56 (9) (2001) 2901–2920.
[36] R.M. German, Prediction of sintered density for bimodal powder mixtures, Metall. Trans. A. 23 (5) (1992) 1455–1465.
[37] S.P. Usher, Suspension Dewatering: Characterisation and Optimisation, University of Melbourne (Australia), 2002.
[38] R.G. de Kretser, S.P. Usher, P.J. Scales, D.V. Boger, K.A. Landman, Rapid filtration measurement of dewatering design and optimization parameters, AICHE J. 47 (8) (2001) 1758–1769.
[39] D.T. Fisher, S.A. Clayton, D.V. Boger, P.J. Scales, The bucket rheometer for shear stress-shear rate measurement of industrial suspensions, J. Rheol. 51 (5) (2007) 821–831.
[40] A.D. Stickland, R.G. de Kretser, P.J. Scales, S.P. Usher, P. Hillis, M.R. Tillotson, Numerical modelling of fixed-cavity plate-and-frame filtration: formulation, validation and optimisation, Chem. Eng. Sci. 61 (12) (2006) 3818–3829.
[41] E. Höfgen, D. Collini, R.J. Batterham, P.J. Scales, A.D. Stickland, High pressure dewatering rolls: comparison of a novel prototype to existing industrial technology, Chem. Eng. Sci. 205 (2019) 106–120.
[42] R. Sivamohan, E. Forssberg, Recovery of heavy minerals from slimes, Int. J. Miner. Process. 15 (4) (1985) 297–314.
[43] M. Alderliesten, Mean Particle Diameters, Part II: standardization of nomenclature, Part. Part. Syst. Charact. 8 (1–4) (1991) 237–241.
[44] S.P. Usher, R.G. de Kretser, P.J. Scales, Validation of a new filtration technique for dewaterability characterisation, AICHE J. 47 (7) (2001) 1561–1570.
[45] D.R. Lester, S. Usher, P.J. Scales, Estimation of the hindered settling function R(ϕ) from batch settling tests, AICHE J. 51 (2005) 1158–1168.
[46] G.J. Kynch, A theory of sedimentation, Trans. Faraday Soc. 48 (0) (1952) 166–176.
[47] S.P. Usher, L.J. Studer, R.C. Wall, P.J. Scales, Characterisation of dewaterability from equilibrium and transient centrifugation test data, Chem. Eng. Sci. 93 (2013) 277–291.
[48] Q.D. Nguyen, D.V. Boger, Yield stress measurement for concentrated suspensions, J. Rheol. 27 (4) (1983) 321–349.
[49] A.D. Stickland, A. Kumar, T.E. Kusuma, P.J. Scales, A. Tindley, S. Biggs, R. Buscall, The effect of premature wall yield on creep testing of strongly flocculated suspensions, Rheol. Acta 54 (5) (2015) 337–352.
[50] A.D. Stickland, R. Buscall, Whither compressional rheology? J. Non-Newtonian Fluid Mech. 157 (3) (2009) 151–157.
[51] Z. Zhou, M.J. Solomon, P.J. Scales, D.V. Boger, The yield stress of concentrated flocculated suspensions of size distributed particles, J. Rheol. 43 (3) (1999) 651–671.
[52] R. Buscall, P.D.A. Mills, J.W. Goodwin, D.W. Lawson, Scaling behaviour of the rheology of aggregate networks formed from colloidal particles, J. Chem. Soc., Faraday Trans. 1: Phys. Chem. Condens. Phases 84 (12) (1988) 4249–4260.
[53] E. Höfgen, H.-E. Teo, P.J. Scales, A.D. Stickland, Vane-in-a-filter and vane-under-compressional-loading: novel methods for the characterisation of combined shear and compression, Rheol. Acta 59 (6) (2020) 349–363.
[54] G.M. Channell, C.F. Zukoski, Shear and compressive rheology of aggregated alumina suspensions, AICHE J. 43 (7) (1997) 1700–1708.
[55] R. Buscall, P.D.A. Mills, R.F. Stewart, D. Sutton, L.R. White, G.E. Yates, The rheology of strongly-flocculated suspensions, J. Non-Newtonian Fluid Mech. 24 (2) (1987) 183–202.
[56] D.R. Lester, R. Buscall, A.D. Stickland, P.J. Scales, Wall adhesion and constitutive modeling of strong colloidal gels, J. Rheol. 58 (5) (2014) 1247–1276.
[57] G. Bickert, A. Vince, Improving vacuum filtration by chemical and mechanical means, in: Proceedings of the Thirteenth Australian Coal Preparation Conference, 2010. Mackay, Queensland.
[58] S. Illies, J. Pfinder, H. Anlauf, H. Nirschl, Filter cake compaction by oscillatory shear, Drying Technol. 35 (1) (2017) 66–75.
[59] P. Menesklou, T. Sinn, H. Nirschl, M. Gleiss, Scale-up of decanter centrifuges for the particle separation and mechanical dewatering in the minerals processing industry by means of a numerical process model, Minerals 11 (2) (2021) 229.
[60] P. Menesklou, H. Nirschl, M. Gleiss, Dewatering of finely dispersed calcium carbonate-water slurries in decanter centrifuges: about modelling of a dynamic simulation tool, Sep. Purif. Technol. 251 (2020) 117287.
[61] Y. Zhang, P. Grassia, A. Martin, S.P. Usher, P.J. Scales, Mathematical modelling of batch sedimentation subject to slow aggregate densification, Chem. Eng. Sci. 128 (2015) 54–63.
[62] R. Seto, R. Botet, M. Meireles, G. Auernhammer, B. Cabane, Compressive consolidation of strongly aggregated particle gels, J. Rheol. 57 (2013) 1347.
[63] R. Buscall, P.J. Scales, A.D. Stickland, H.-E. Teo, D.R. Lester, Dynamic and rate-dependent yielding in model cohesive suspensions, J. Non-Newtonian Fluid Mech. 221 (2015) 40–54.
[64] T.E. Kusuma, P.J. Scales, R. Buscall, D.R. Lester, A.D. Stickland, Strain softening of concentrated cohesive particulate suspensions prior to yield, J. Rheol. 65 (3) (2021) 355–370.
[65] A.D. Stickland, R.G. de Kretser, A.R. Kilcullen, P.J. Scales, P. Hillis, M.R. Tillotson, Numerical modeling of flexible-membrane plate-and-frame filtration, AICHE J. 54 (2) (2008) 464–474.
[66] A. Stickland, E. Irvin, S. Skinner, P. Scales, A. Hawkey, F. Kaswalder, Filter press performance for fast-filtering compressible suspensions, Chem. Eng. Technol. 39 (2016) 409–416.
[67] Diemme Filtration, GHT5000F Domino, 5th Feb 2024]; Available from, https://www.diemmefiltration.com/filterpress-for-sludge/filter-press-ght-5000f-domino/, 2022.
[68] S. Hassan, N.I.K. Ekanayake, P.J. Scales, R.J. Batterham, A.D. Stickland, High pressure dewatering rolls Mk-II: a novel dewatering technology for mineral tailings, in: FILTECH 2023 Conference Proceedings, 2023. Cologne, Germany.